

Infrared spectrum of single-walled boron nitride nanotubes

B. Fakrach, A. Rahmani, H. Chadli, K. Sbai, and M. Bentalab

Laboratoire de Physique des matériaux et Modélisation des Systèmes, Université Moulay Ismail, Faculté des Sciences (Unité Associée au CNRST-URAC08), Boîte Postale 11201, Zitoune, 50000 Meknès, Morocco

J.-L. Bantignies and J.-L. Sauvajol

Laboratoire des Colloïdes, Verres et Nanomatériaux (UMR CNRS 5587), CP026, Université Montpellier II, 34095 Montpellier Cedex 5, France

(Received 18 June 2011; revised manuscript received 12 February 2012; published 26 March 2012)

Using the spectral moment's method, the infrared spectra of single-walled boron nitride nanotubes are calculated. The dependence of these modes has been calculated as a function of the nanotube chirality, diameter (from 0.7 to 5 nm), and length. These predictions are useful for understanding the experimental infrared spectra of boron nitride nanotubes.

DOI: [10.1103/PhysRevB.85.115437](https://doi.org/10.1103/PhysRevB.85.115437)

PACS number(s): 61.46.Fg, 61.43.Bn

I. INTRODUCTION

Since their discovery, carbon nanotubes (CNTs)¹ and boron nitride nanotubes (BNNTs)² have been receiving an ever-increasing interest due to their particular properties and potential application in nanodevices.^{3–5} In contrast to CNTs, which can be either semiconducting or metallic, depending on the chirality of the tube and diameter,^{6,7} BNNTs are always semiconducting. The band gap of a BNNT was theoretically predicted to be approximately equal to that of *h*-BN (around 5 eV) independent of their diameter, chirality, and wall numbers.^{8,9} However, recent experiments have shown that this band gap was higher than 5.5 eV.¹⁰ The stability of BNNTs was first predicted based on tight-binding⁸ and first-principles⁹ calculations.

A variety of growing methods, such as arc discharge,^{2,11,12} laser ablation,^{13,14} ball milling,^{15,16} chemical vapor deposition (CVD),^{17–20} and substitution reaction,²¹ were developed to synthesize multiwalled boron nitride nanotubes (MBNNTs). Recently, Lee *et al.*²² have prepared MBNNTs by thermal chemical vapor deposition. The diameters of the MBNNTs prepared by this route were evaluated by scanning electron microscopy. They range from 10 to 100 nm, depending on the growing parameters, and their length is estimated to be longer than 10 μm . More recently, Guo *et al.*²³ showed that MBNNTs appear in bundles with a width close to 50–70 nm or as a single tube with a diameter around 5–20 nm.

By contrast to CNTs for which Raman resonance conditions are achieved in the visible and IR range, Raman spectroscopy is not an easy tool to characterize BNNTs because their resonance conditions occurs in the UV range. Due to the existence of a dipolar moment between N and B atoms, IR spectroscopy can be used to characterize BNNTs. In MBNNT samples, the IR spectrum shows two main absorption bands located around 805–815 and 1369–1390 cm^{-1} . The position of the IR modes in each range is sample dependent (see Table I). The mode in the 1369–1390 cm^{-1} band originates from the in-plane stretching modes of *h*-BN networks. The weak absorption in the 805–815 cm^{-1} range is associated with the out-of-plane radial buckling (R) mode where boron and nitrogen atoms are moving radially inward or outward. Up to now, no experimental evidence of infrared-active modes has been reported in the far-IR region.

In this paper we focus on the infrared-active modes of single-walled boron nitride nanotubes (SBNNTs). The structures of the armchair, zigzag, and chiral nanotubes are described by the symmetry groups C_{2nh} , C_{2nv} , and C_N , respectively.²⁷ Group-theoretical analysis^{27,28} reveals that four A and five E_1 modes for a chiral SBNNT ($\Gamma_{\text{ir}}^{\text{chi}} = 4A \oplus 5E_1$), three A_1 and five E_1 modes for a zigzag SBNNT ($\Gamma_{\text{ir}}^{\text{zig}} = 3A_1 \oplus 5E_1$), and one A_u and three E_{1u} modes for an armchair SBNNT ($\Gamma_{\text{ir}}^{\text{arm}} = A_u \oplus 3E_{1u}$) are infrared active.

The phonons of individual SBNNTs have been calculated with different approaches: valence-shell model,²⁸ tight-binding approach,²⁹ force-constant model,³⁰ and *ab initio* calculations.^{31–33} It must be emphasized that these approaches do not permit us to calculate the phonons in SBNNT with a large diameter or finite length due to the significant number of atoms, which is necessary to take into account. The spectral moments method (SMM) is an alternative way to solve this latter problem. The moments method was initially developed by different authors studying electronic properties in solid-state physics.^{34,35} A few years ago, the SMM was shown to be a powerful tool for determining infrared absorption, Raman scattering, and inelastic neutron-scattering spectra of harmonic systems.^{36–40} This method can be applied to large systems, whatever the type of atomic forces, the spatial dimension, and structure of the material. This method was previously used to study the dynamical properties of different disordered systems having more than 10^6 degrees of freedom, as is the case with Sierpinski gaskets,³⁷ silica aerogels,³⁸ and diffusion-limited cluster-cluster aggregates.^{39,40} The SMM was recently used to calculate IR and Raman spectra of carbon nanotubes^{41–45} and peapods.^{46–48} The nonresonant Raman spectra of SBNNTs have been calculated⁴⁹ using the force-constant model of Xiao *et al.*³⁰ and the spectral moments method³⁶ in the framework of the bond-polarization theory. A good agreement with group theory prediction was found. Particularly, in good agreement with the theoretical results,^{28,30,31} it was shown that the radial breathing-mode wave number is inversely proportional to the nanotube diameters, and no chirality effect is evidenced.

In this paper, we use the spectral moments method to calculate the infrared spectra of individual finite and infinite single-walled boron nitride nanotubes. In Sec. II, we present the structure of SBNNTs, the dynamical model, and the computational

TABLE I. Infrared experimental data in MBNNT.

Reference	IWN	HWN
Ref. 22	800/815	1369
Ref. 24	805	1380
Ref. 25	810	1390
Ref. 26	813	1389

technique. Calculation for SBNNTs with different diameters (0.7–5 nm), chiralities (armchair, zigzag, and chiral), and lengths are reported in Sec. III. In the same section, a comparison between experimental IR data and calculations is reported.

II. MODELS AND COMPUTATIONAL METHOD

A single-walled BN nanotube can be obtained from an h -BN sheet by rolling it up along the straight line connecting two equivalent lattice points into a seamless cylinder in a way that the two points coincide. Following the usual terminology of reference,⁶ the tube can be specified by integers (n, m) , which define the chiral vector between the two points. Alternatively, the tube can be described by its diameter D and the chiral angle θ , which is the angle between the chiral vector and the nearest zigzag of B-N bonds. The SBNNT chirality can be classified into two types: achiral tubes, including armchair (n, n) and zigzag $(n, 0)$ SBNNTs, and chiral SBNNTs $(n, m \neq n \neq 0)$.

To calculate the phonon modes in SBNNT, it is necessary to start from an accurate model which reproduces the phonon dispersion curves of the two-dimensional (2D) hexagonal h -BN layer measured from high-resolution electron energy loss spectroscopy.⁵⁰ By using a Born–von Karman model and by taking into account interactions up to the fourth neighbors both for force constants in the plane and out of plane, Xiao *et al.*³⁰ provide a reasonable description of the experimental phonon dispersion curves of the h -BN layer. In a nanotube, the force-constant matrix between the i and j atoms is obtained by rotating the B-N chemical bond from the two-dimensional plane of h -BN to the three-dimensional cylindrical coordinate system of a nanotube. Infrared absorption measurements performed on multiwalled BN nanotubes show two strong peaks located around 800 and 1380 cm^{-1} (Refs. 20, 22, 24–26). In order to reproduce the experimental position of these IR features, the first-nearest-neighbor force constants of the Xiao model are slightly modified. The modified Xiao force constants are given in Table II, where the subscripts r , t_i , and t_o refer to stretching, in-plane bending, and out-of-plane bending, respectively. No significant changes have been obtained for

TABLE II. Force-constant parameters for 2D h -BN in units of 10^4 dyn cm^{-1} . Here the subscripts r , t_i , and t_o refer to radial, transverse in plane, and transverse out of plane, respectively.

Radial	Tangential	
$\phi_r^1 = 40.50$	$\phi_{t_i}^1 = 9.50$	$\phi_{t_o}^1 = 7.50$
$\phi_r^{B-B} = 7.00$	$\phi_{t_i}^{B-B} = -3.23$	$\phi_{t_o}^{B-B} = -0.70$
$\phi_r^{N-N} = 8.00$	$\phi_{t_i}^{N-N} = -0.73$	$\phi_{t_o}^{N-N} = -0.55$
$\phi_r^3 = 1.00$	$\phi_{t_i}^3 = -3.25$	$\phi_{t_o}^3 = 0.65$
$\phi_r^4 = -1.90$	$\phi_{t_i}^4 = 1.29$	$\phi_{t_o}^4 = -0.30$

(10,10) BNNT phonon dispersion curves with the new set of parameters in comparison with Xiao ones (Fig. 1 of Ref. 30).

The IR absorption spectrum $I_\alpha(\omega)$ is given by⁵¹

$$I_\alpha(\omega) = \frac{\omega}{nc} \sum_j \frac{|a_{j\alpha}|^2}{2\omega_j} [\delta(\omega - \omega_j) - \delta(\omega + \omega_j)], \quad (1)$$

with

$$a_{j\alpha} = \sum_k \frac{q_k}{\sqrt{M_k}} e_j(k\alpha), \quad (2)$$

where n and c are, respectively, the refractive index of the material and the speed of light. q_k is the effective charge tensor, and M_k is the mass of the k th atom. ω_j and $e_j(k\alpha)$ are the wave number and the $(k\alpha)$ component of the displacement amplitude for the k th atom (α is Cartesian coordinate) in the j th mode. A usual method to calculate the IR spectrum consists of injecting in the previous expressions the values of ω_j and $e_j(k\alpha)$ obtained by direct diagonalization of the dynamical matrix \tilde{D} of the system by resolving

$$\tilde{D}|j\rangle = \omega_j^2|j\rangle \quad (3)$$

However, when the system contains a large number of atoms, as for long tubes of finite length, the dynamical matrix \tilde{D} is very large, and its diagonalization fails or requires long computing time. In contrast, the spectral moments method allows us to compute directly the IR spectrum of very large harmonic systems without any diagonalization of the dynamical matrix.^{36,38} Otherwise, for small samples, both approaches lead exactly to the same position and intensity for the different peaks.

Considering the symmetrical function $\Im(\omega)$, where $a(j)$ is given by Eq. (2),

$$\Im(\omega) = \sum_j \frac{|a(j)|^2}{2\omega_j} [\delta(\omega - \omega_j) + \delta(\omega + \omega_j)]. \quad (4)$$

This function is identical (for $\omega > 0$), apart from constants, to a component of the IR absorption [Eq. (1)] for a given polarization. The response of the system is given by the function $\Im(\omega)$, which can be further written as

$$J(u) = \sum_j |a(j)|^2 \delta(u - \lambda_j), \quad (5)$$

where $u = \omega^2$ and $\lambda_j = \omega_j^2$.

$J(u)$ can be directly carried out from the dynamical matrix \tilde{D} and from the effective charge tensor, without any diagonalization. In fact, it is easy to show that

$$J(u) = -\frac{1}{\pi} \lim_{\epsilon \rightarrow 0^+} \text{Im}[R(z)], \quad (6)$$

where $z = u + i\epsilon$ and $R(z) = \langle q | (z\tilde{I} - \tilde{D})^{-1} | q \rangle$. The (δn) component of the $|q\rangle$ vector is given by the expression

$$\langle \delta n | q \rangle = \frac{q_n}{\sqrt{M_n}}, \quad (7)$$

which is supposed to be known for a given (δ) component of the IR absorption.

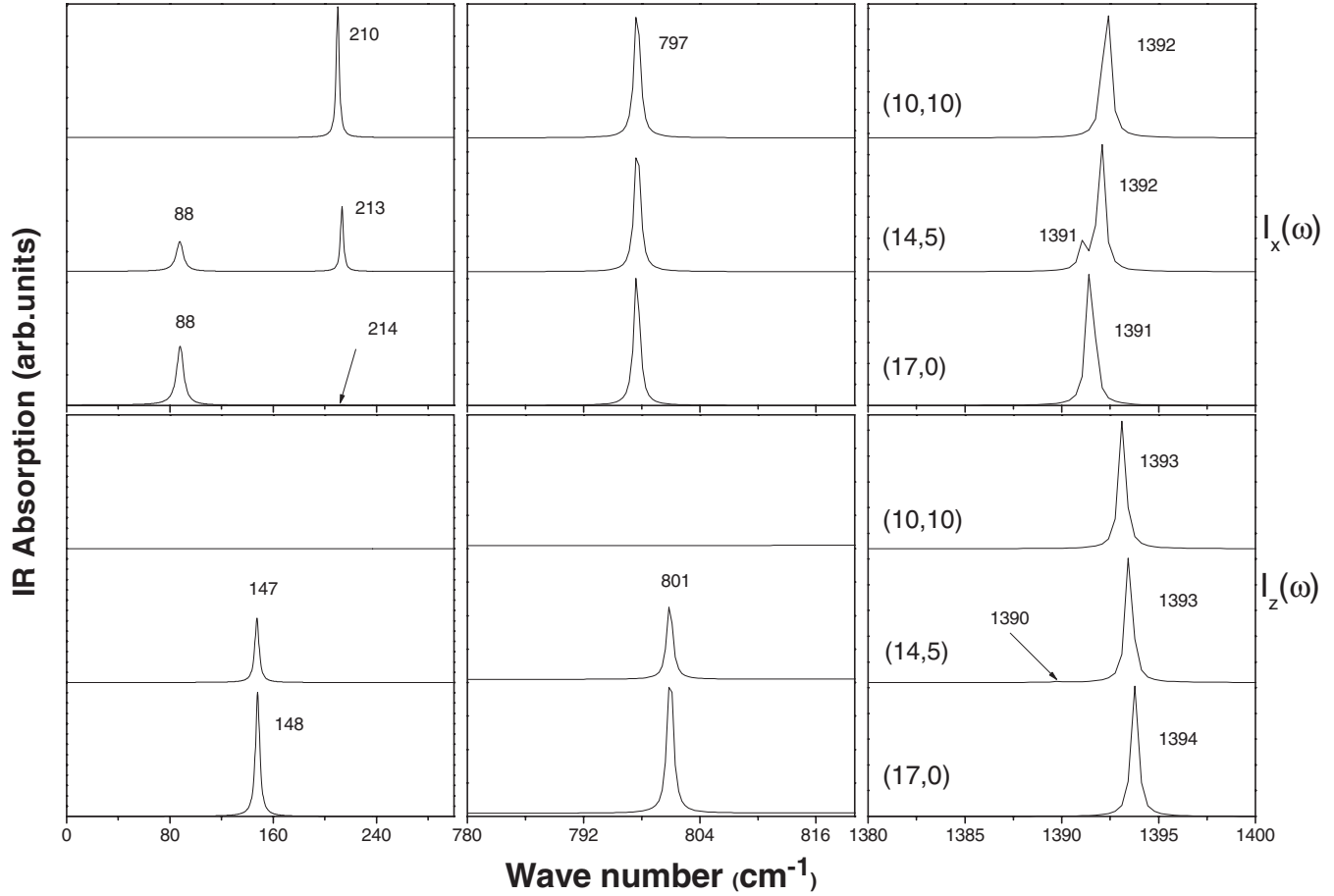


FIG. 1. The (bottom) $I_z(\omega)$ and (top) $I_x(\omega)$ polarized infrared spectra calculated for a (10,10), (14,5), and (17,0). Spectra are displayed in the (left) low-, (middle) intermediate-, and (right) high-wave-number regions.

The spectral moments method consists of developing $R(z)$ in a continued fraction:

$$R(z) = \frac{b_0}{z - a_1 - \frac{b_1}{z - a_2 - \frac{b_2}{z - a_3 - \dots}}}, \quad (8)$$

where the coefficients a_n and b_n are given by

$$a_{n+1} = \bar{\nu}_{nn}/\nu_{nn}; \quad b_n = \nu_{nn}/\nu_{n-1n-1}; \quad b_0 = 1. \quad (9)$$

The spectral generalized moments ν_n and $\bar{\nu}_n$ of $J(u)$ are directly obtained from the dynamical matrix \tilde{D} .

$$\nu_{nn} = \langle q_n | q_n \rangle; \quad \bar{\nu}_{nn} = \langle q_n | \tilde{D} | q_n \rangle, \quad (10)$$

with

$$\begin{aligned} |q_{n+1}\rangle &= (\tilde{D} - a_{n+1})|q_n\rangle - b_n|q_{n-1}\rangle; \\ |q_{-1}\rangle &= 0; \quad |q_0\rangle = 1. \end{aligned} \quad (11)$$

Iterations enable the computation of expression (8) and then the function $I(\omega)$. Each element of the dynamical matrix \tilde{D} is given by

$$D_{\alpha\beta}(n,m) = \frac{1}{\sqrt{M_n M_m}} \phi_{\alpha\beta}(n,m), \quad (12)$$

with $\phi_{\alpha\beta}(n,m)$ being the force constants between n and m atoms.

The wave numbers of the infrared-active modes were directly obtained from the position of the peaks in the calculated IR spectra. In all the following calculations, the line shape of each peak is assumed to be Lorentzian, and the width is fixed at 1.7 cm^{-1} .

The IR intensity depends on the dynamic dipolar moment variation (or effective charge ratio q_B/q_N) between nitrogen and boron atoms for BNNTs systems. In the literature and to the best of our knowledge, there is no calculation of the effective charge on SBNNT. In this work, in order to enhance the IR response of nanotubes, effective charges on boron and nitrogen atoms are fixed at $q_B = +1$ and $q_N = -1$ for a given B-N bond. Consequently, the intensities obtained in this work cannot be compared to the experimental spectra. However, these results can be used to analyze the dependence in intensity of a mode with diameter or chirality. Finally, the SMM predictions concerning the number and position of IR lines as a function of diameter, length, and chirality do not depend on the charge ratio q_B/q_N , and the SMM predictions can help to interpret the IR experimental data.

III. RESULTS AND DISCUSSION

We report the calculations of the infrared responses of achiral and chiral SBNNTs of different diameters and lengths. In all the calculations, the nanotube axis is along the Z axis.

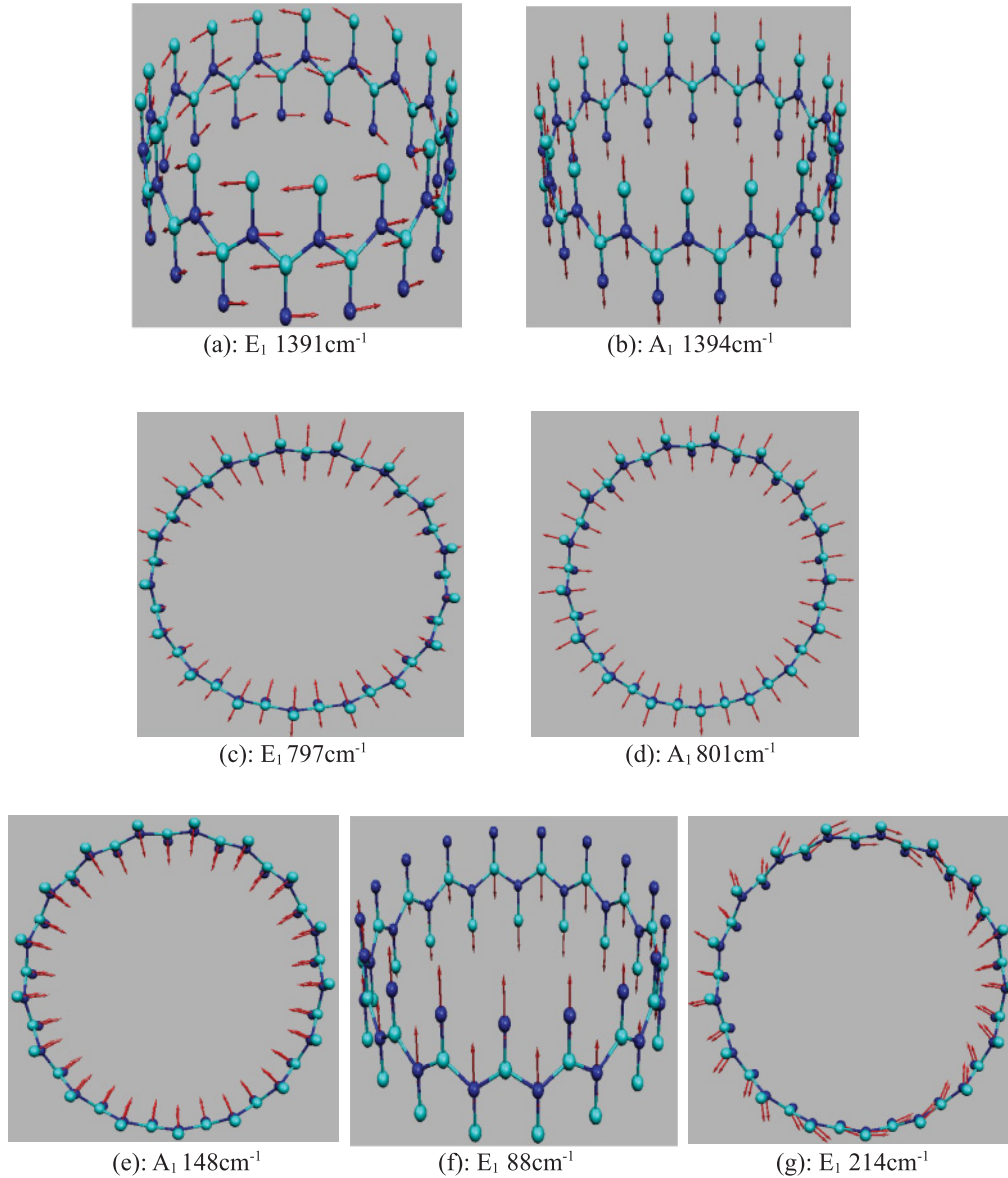


FIG. 2. (Color online) Infrared-active-mode atomic displacements and symmetries for selected normal modes in the (17,0) SBNNT.

A. Symmetry of the IR-active modes

Calculations are first performed on infinite SBNNTs which are obtained by applying periodic conditions on the unit cells of the nanotube. The symmetries of the infrared-active modes are directly derived from the polarized $I_Z(\omega)$ and $I_X(\omega)$ spectra. Indeed, it was established that the A_u (E_{1u}) IR mode of an armchair SBNNT, the A_1 (E_1) IR modes of zigzag SBNNT, and the A (E_1) IR modes of chiral SBNNTs are active in the $I_Z(\omega)$ [$I_X(\omega)$] spectrum.²⁷ The $I_Z(\omega)$ and $I_X(\omega)$ spectra of (10,10), (14,5), and (17,0) SBNNTs are displayed in Fig. 1.

In the high-wave-number (HWN) range, above 1200 cm^{-1} , the $I_X(\omega)$ and $I_Z(\omega)$ polarized spectra are dominated by strong IR-active modes. The $I_X(\omega)$ spectra show that the E_{1u} mode is calculated around 1392 cm^{-1} in (10,10) armchair SBNNT, the two E_1 modes, located around 1391 cm^{-1} , are accidentally degenerated in the (17,0) zigzag SBNNT, and the two E_1 modes are found at 1391 and 1392 cm^{-1} in the spectrum

of the (14,5) SBNNT. The $I_Z(\omega)$ spectra evidence that the A_u mode is located at 1393 cm^{-1} for the (10,10) armchair SBNNT, and the A_1 mode is found at 1394 cm^{-1} for the (17,0) tube. For the (14,5) chiral nanotube, two A_1 modes located around 1390 cm^{-1} (with a very weak intensity) and 1393 cm^{-1} are predicted.

The eigenvector displacements of the modes of (17,0) SBNNT are given in Fig. 2 (the arrows indicate the magnitude and direction of B and N atom displacements). These vectors allow us to identify the longitudinal or transverse character of the optical modes. In the HWN range, all the modes are tangential modes. With respect to the tube axis, the strong E_1 mode is a transverse optical mode [Fig. 2(a)], and the E_1 mode, with a weak intensity, and the A_1 mode [Fig. 2(b)] are longitudinal optical modes. Also, as evidenced from their eigenvector displacements (not shown), in the (14,5) chiral SBNNT, the E_1 mode, close to 1391 cm^{-1} , is a longitudinal optical mode, and the strong mode at 1392 cm^{-1} is a transverse one.

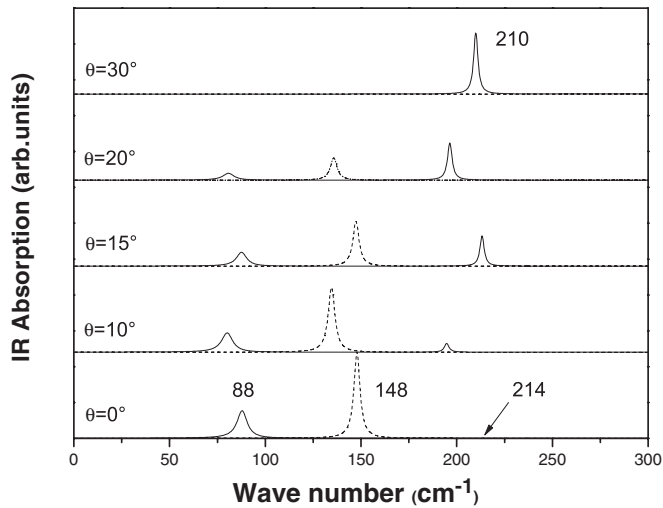


FIG. 3. Dependence of the low-wave-number infrared spectrum as a function of the chiral angle θ : $I_Z(\omega)$ (dashed line) and $I_X(\omega)$ (solid line). All the spectra are displayed with the same intensity scale.

Concerning the intermediate-wave-number (IWN) region, from 600 to 1200 cm^{-1} , independently of the SBNNT chirality, the $I_X(\omega)$ spectrum is dominated by a strong single mode located around 797 cm^{-1} of E_{1u} (E_1) symmetry for armchair

(zigzag and chiral) SBNNTs. This mode corresponds to an out-of-plane mode with radial displacements of B and N atoms in the opposite directions, as illustrated in Fig. 2(c). There are two nodes along the circumference and all boron atoms move inward (outward), while all nitrogen atoms move outward (inward) on both sides of the nodes. In good agreement with theoretical results,^{28,29,31-33} no IR-active mode appears for the armchair tube in the $I_Z(\omega)$ spectrum. A single mode of A_1 (A) symmetry, located around 801 cm^{-1} , was found for the (17,0) zigzag [(14,5) chiral]. As shown in Fig. 2(d), this mode is an out-of-plane mode with radial displacements of B and N atoms in the opposite directions: all boron atoms move inward (outward) when all nitrogen atoms move outward (inward).

In the low-wave-number (LWN) range ($<600 \text{ cm}^{-1}$), the $I_Z(\omega)$ spectrum shows a single mode (A_1 symmetry) centered at 148 cm^{-1} for the (17,0) tube and a mode (A symmetry) for the (14,5) tube. No mode is calculated for the (10,10) armchair tube. This mode is assigned to the radial breathing mode (RBM) of the tube, and all atoms in the unit cell move in phase in the radial direction [Fig. 2(e)]. Our calculations confirm that this RBM is only IR active for chiral and zigzag tubes, in good agreement with tight-binding²⁹ and *ab initio*^{31,32} calculations.

In the $I_X(\omega)$ spectrum, two E_1 modes located around 88 and 214 cm^{-1} are predicted for (14,5) and (17,0) SBNNTs, and a single E_{1u} mode at 210 cm^{-1} is calculated for the (10,10) armchair tube. The E_1 (88 cm^{-1}) mode corresponds

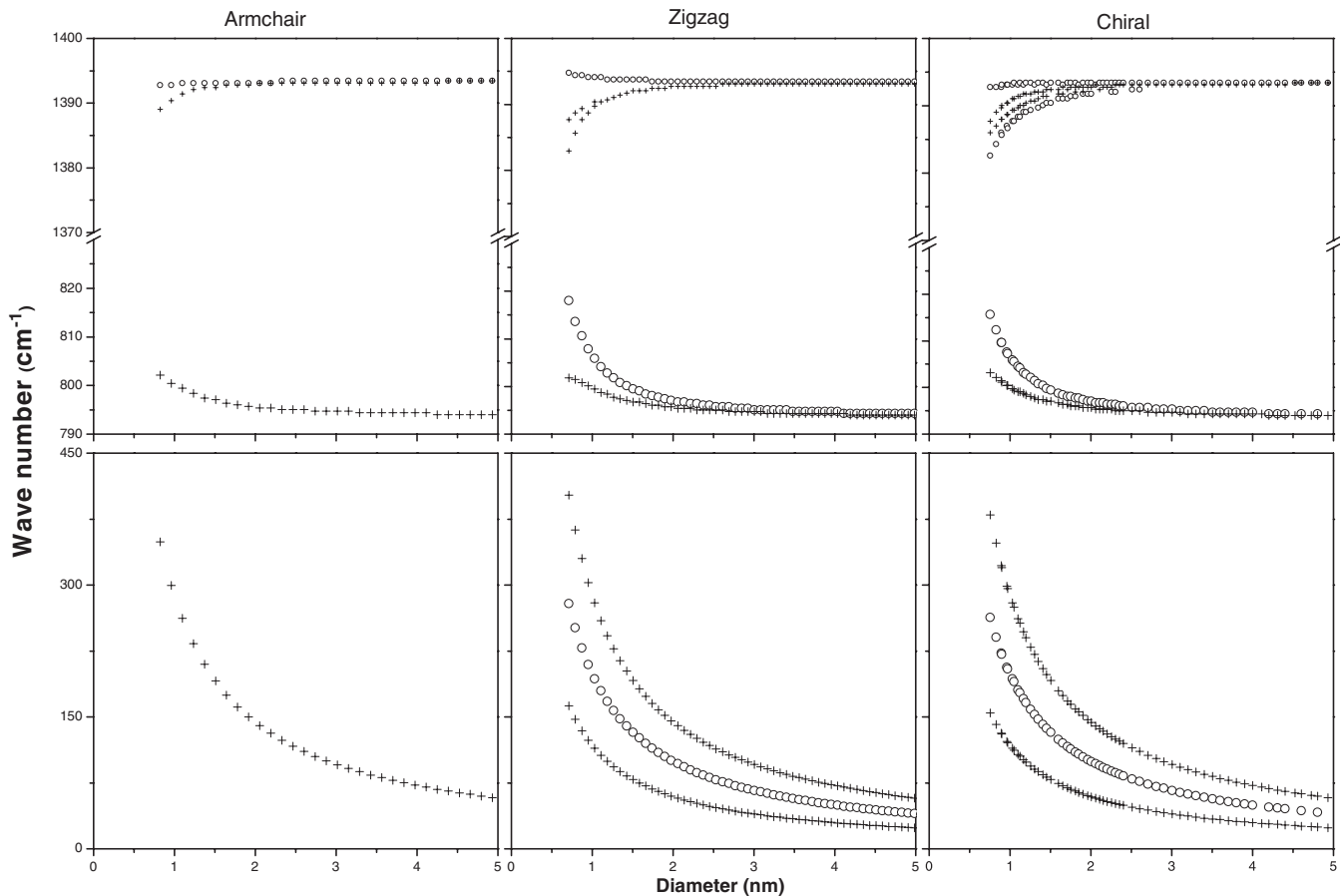


FIG. 4. Diameter dependence of the wave numbers of the main infrared-active modes of SBNNTs: modes observed in the $I_Z(\omega)$ spectrum (circles) and modes observed in the $I_X(\omega)$ spectrum (crosses).

TABLE III. The a , b , and c parameters for the a/D and $a/D + b/D^2 + c$ dependences of the modes as a function of the tube diameter D . Units are as follows: a , nm cm⁻¹; b , nm² cm⁻¹; c , cm⁻¹.

Range	Mode Symmetry	Parameters	Zigzag	Armchair	Chiral
LWN	A		198.71		198.53
	E^l	a	116.60		116.88
	E^h	a	287.05	286.77	287.16
IWN	A	a	2.03		1.94
		b	11.20		11.38
		c	793.22		793.22
	E	a	9.17	7.32	5.51
		b	-1.00	0.85	2.11
		c	791.30	791.81	792.37
HWN	A^l	a			-0.29
		b			-5.87
		c			1393.38
	A^h	a	0.75	-0.68	0.84
		b	0.34	-0.056	-0.92
		c	1393.02	1393.61	1393.20
	E^l	a	7.09	5.38	-0.63
		b	-9.21	-6.57	-3.93
		c	1391.37	1391.94	1393.63
	E^h	a	-0.11		3.84
		b	-2.57		-5.41
		c	1393.92		1392.26

to a longitudinal mode with B and N atoms moving upward (downward) on both sides of the nodes [Fig. 2(f)]. The E_1 mode at 214 cm⁻¹ corresponds to a mixing of tangential and radial displacement of B and N atoms, as shown in Fig. 2(g). There are two nodes along the circumference, and all boron and nitrogen atoms move inward (outward) for the radial component and upgrade (downgrade) for the tangential one on both sides of the two nodes.

To illustrate the chirality dependence of the infrared-active modes in the low-wave-number range, the calculated $I_X(\omega)$ and $I_Z(\omega)$ spectra are displayed for five values of the chiral angle θ (0°, 10°, 15°, 20°, and 30°), associated with (17,0), (17,3), (14,5), (14,7), and (10,10) SBNNTs, respectively (Fig. 3). We observe for both polarized infrared spectra an oscillatory wave number behavior of the modes which is related to the variations in the diameter of the selected SBNNTs: 1.35 nm (17,0), 1.48 nm (17,3), 1.35 nm (14,5), 1.47 nm (14,7), and 1.37 nm (10,10). On the $I_Z(\omega)$ spectrum (dashed lines), the increase of θ from 0° (zigzag) to 30° (armchair) leads to the progressive vanishing of the mode located around 148 cm⁻¹, and for $\theta = 30^\circ$ no mode was observed. In the $I_X(\omega)$ spectrum (solid lines) of zigzag SBNNT a strong mode is calculated at 88 cm⁻¹ and a small one is calculated at 214 cm⁻¹. The increase of θ from 0° to 30° leads to the rise of the intensity of the high-frequency mode by contrast with the vanishing of the low-frequency mode.

B. Diameter and length dependence of the active modes

Figure 4 shows the diameter dependence of the wave numbers of the IR-active modes (circles for A modes and crosses for E modes) for armchair (left), zigzag (middle),

and chiral (right) SBNNTs. In the LWN and IWN ranges, independent of the chirality, all the modes downshift with increasing tube diameter. By contrast, in the HWN region, all the modes upshift when the tube diameter increases, except the A_1 tangential mode of zigzag SBNNTs, which slightly downshift when the diameter increases. One can see that the LWN modes are strongly dependent on the diameter in comparison with HWN and IWN modes. From these results, and for SBNNTs in the diameter range 0.7–2.5 nm, phenomenological relations which describe the diameter dependence of the IR-active-mode wave numbers have been derived.

In the HWN and IWN regions, we found that the diameter dependence of the totally symmetrical A mode and degenerate E mode wave numbers are well fitted by the phenomenological relation:

$$\omega = a/D + b/D^2 + c, \quad (13)$$

where D is the nanotube diameter. The a , b , and c parameters are given in Table III for armchair, zigzag, and chiral nanotubes. It must be emphasized that this previous expression has a useful application for deriving the diameter of tubes from the experimental infrared-active-mode wave numbers. No physical meaning is attached to the values of the different parameters of the fit.

For large diameters ($D > 2.5$ nm) and independent of chirality, one can observe that all IWN modes overlap, and a result is a single band with a wave number of 793 cm⁻¹ close to the out-of-plane radial buckling mode. All HWN tangential modes also overlap for large diameters to give a

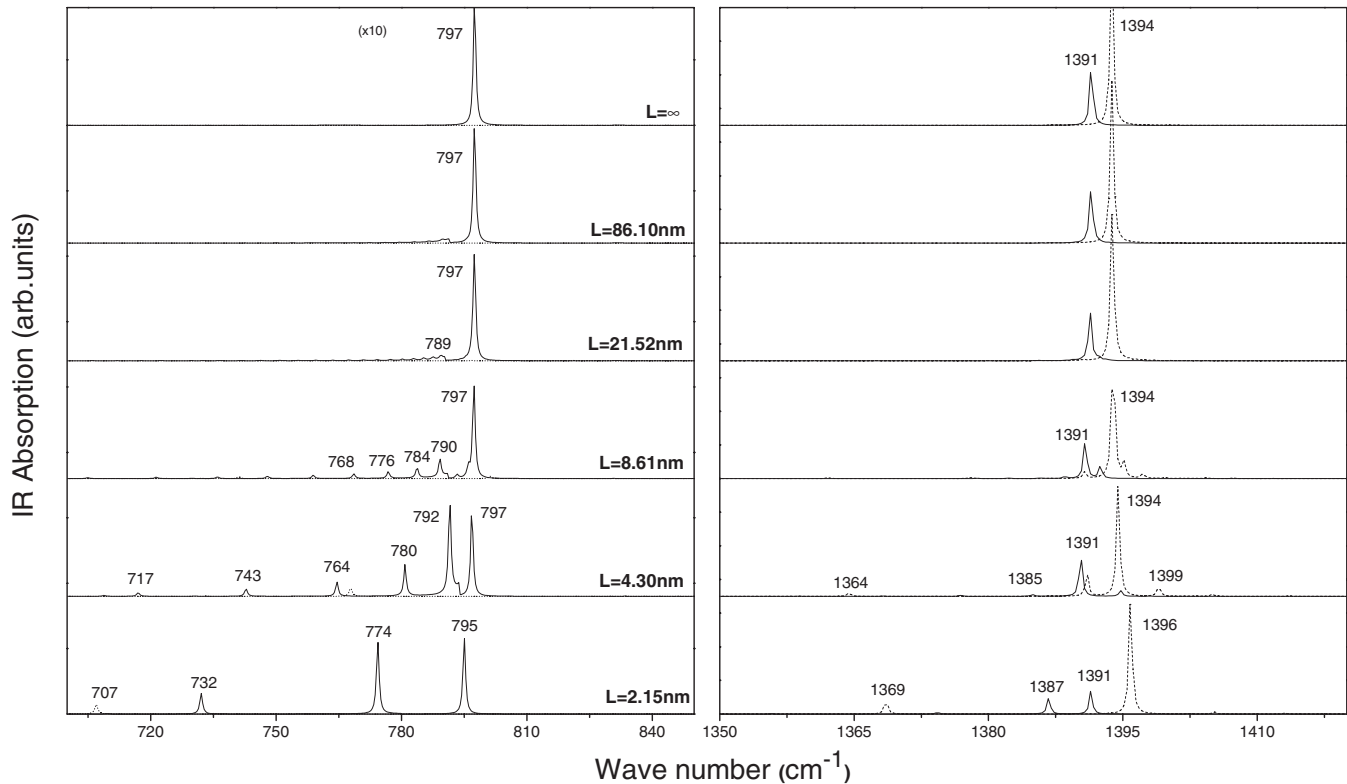


FIG. 5. Dependence of the $I_x(\omega)$ (solid line) and $I_z(\omega)$ (dashed line) (left) IWN and (right) HWN infrared spectra of (17,0) tube as a function of the tube length. Spectra are displayed for five finite lengths, $L = 2.15, 4.30, 8.61, 21.52, 86.10$ nm, and for infinite SBNNT, from bottom to top. All the spectra are displayed with the same intensity scale.

single band with a wave number of 1393 cm^{-1} close to the in-plane stretching mode of h -BN.

In the LWN range, the dependence of the wave number of the A and E modes as a function of tube diameter is described by an a/D scaling law with the a parameter depending on the mode symmetry (see Table III). The value of this latter parameter is close to 116, 198, and 287 nm cm^{-1} for the lowest E (E^l) mode, RBM, and highest E (E^h) mode, respectively, independent of chirality. This behavior is close to the one calculated for the Raman-active breathing modes using the same approach⁴⁹ and *ab initio* methods.^{28,29,31-33} Our fitting constants for RBM are consistent with the values of 205 and 209.8 nm cm^{-1} obtained by Akdim *et al.*³³ for the zigzag and armchair tubes, respectively. In comparison with carbon nanotubes for which a similar a/D trend has been obtained,^{33,47,52} the values of the a parameter are greater than those found in SBNNTs.

Finally, a great advantage of our method is to allow the calculations of the IR spectrum for SBNNTs of finite lengths. The calculated infrared spectra of finite SBNNTs, with open ends, have been calculated. These spectra show the same behavior as a function of the nanotube length, independent of chirality. To illustrate the length dependence of the IR spectrum, results for the (17,0) SBNNT are shown in Fig. 5 in the IWN (left) and HWN (right) regions. As expected, additional modes are observed for small tube lengths. Our calculations also state that the IR spectra of a 90-nm-length nanotube is very close to those calculated for an infinite SBNNT. Because the length of the majority of BNNTs tubes is

larger than 100 nm, calculations performed for infinite BNNTs can be used to understand the experimental results.

Most of the infrared experiments are performed on unoriented MBNNT samples. To make the comparison with the experimental results as realistic as possible, we performed an average of the infrared spectra over the nanotube orientations with regard to the laboratory frame. In Fig. 6,

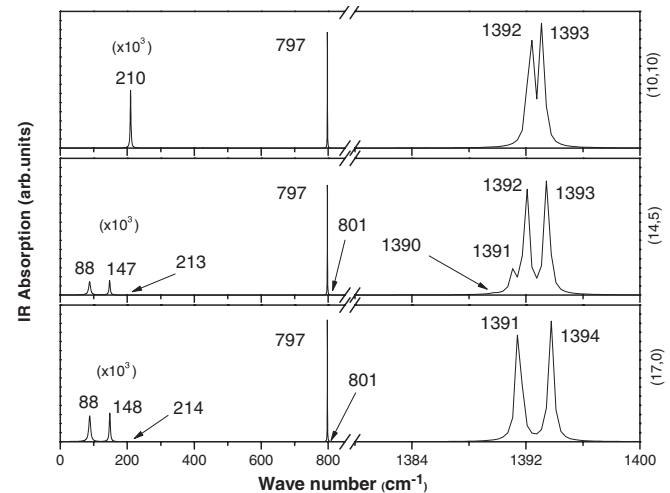


FIG. 6. Average infrared spectra (unoriented sample) calculated for (top) (10,10), (middle) (14,5), and (bottom) (17,0) SBNNTs. All the spectra are displayed with the same intensity scale.

we present the IR spectra calculated for unoriented samples of (10,10), (14,5), and (17,0) SBNNTs. As expected from symmetry considerations,^{27,28} we have obtained one A_u and three E_{1u} modes for the armchair SBNNT, three A_1 and five E_1 modes for the zigzag SBNNT, and four A and five E_1 modes for the chiral SBNNT. Figure 6 shows that for the tangential modes ($>1200\text{ cm}^{-1}$), the IR spectrum profile of SBNNT is sensitive to the chirality, with broader bands expected for chiral and zigzag SBNNTs in comparison with the armchair SBNNT. In this range, the three spectra are dominated by modes located at $1390\text{--}1395\text{ cm}^{-1}$. The intermediate region (from 600 to 1200 cm^{-1}) is dominated by a strong peak located around 800 cm^{-1} for all chiralities. Concerning the low-wave-number range ($<600\text{ cm}^{-1}$), one can observe that the IR spectra profile depends on the chirality of the nanotubes with a narrow single peak for the armchair nanotube and three peaks for other chiralities.

As noted in the Introduction, only a few experimental IR spectra have been measured on MBNNTs. Assuming no coupling between the layers, we can compare these data with our calculations performed on SBNNTs. In agreement with our calculations, the spectra exhibit two main bands located around 810 and 1390 cm^{-1} (Refs. 25 and 26). The experimental broadening of the band centered around 1390 cm^{-1} can be related to the distribution of peaks calculated in this range (Fig. 6); by contrast, the narrow band measured around 810 cm^{-1} is in agreement with the presence of a narrow single peak around 801 cm^{-1} in the calculated spectra of Fig. 6.

IV. CONCLUSION

In this paper, using the spectral moments method, calculations of the infrared spectra of single-wall boron nitride nanotubes are reported and discussed. Particularly, the polarized infrared spectra for achiral and chiral SBNNTs are calculated in a large range of diameters and lengths. In agreement with group theory, our calculations predict four, eight, and nine IR-active modes for armchair, zigzag, and chiral SBNNTs, respectively. The behavior of the infrared-active modes as a function of the tube diameter has been analyzed in detail. The diameter dependence of the positions of the modes in the low- and intermediate-wave-number ranges are well fitted with a phenomenological expression. Our calculations suggest a slight dependency of far-infrared modes on the chirality. Like in single-walled carbon nanotubes, $\omega \propto D^{-1}$ dependence has been obtained for IR modes in the far-infrared range; however, their dependence is lower. The finite-size effects are shown to be significant only for short tubes (L less than 80 nm), and the main effect of the length shortening is the appearance of additional peaks in the far and intermediate infrared domain. All these predictions are useful for understanding the experimental infrared spectra of boron nitride nanotubes.

ACKNOWLEDGMENTS

The work was supported by the CNRS-France/CNRST-Morocco agreement.

-
- ¹S. Iijima, *Nature (London)* **354**, 56 (1991).
²N. G. Chopra, R. J. Luyken, K. Cherrey, V. H. Crespi, M. L. Cohen, S. G. Louie, and A. Zettl, *Science* **266**, 966 (1995).
³E. Hernandez, C. Goze, P. Bernier, and A. Rubio, *Phys. Rev. Lett.* **80**, 4502 (1998).
⁴S. Berber, Y. K. Kwon, and D. Tomanek, *Phys. Rev. Lett.* **84**, 4613 (2000).
⁵P. Kim, L. Shi, A. Majumdar, and P. L. McEuen, *Phys. Rev. Lett.* **87**, 215502 (2001).
⁶R. Saito, M. Fujita, G. Dresselhaus, and M. S. Dresselhaus, *Phys. Rev. B* **46**, 1804 (1992).
⁷N. Hamada, S. I. Sawada, and A. Oshiyama, *Phys. Rev. Lett.* **68**, 1579 (1992).
⁸A. Rubio, J. L. Corkill, and M. L. Cohen, *Phys. Rev. B* **49**, 5081 (1994).
⁹X. Blase, A. Rubio, S. G. Louie, and M. L. Cohen, *Europhys. Lett.* **28**, 335 (1994).
¹⁰P. Jaffrennou, J. Barjon, T. Schmid, L. Museur, A. Kanaev, J. S. Lauret, C. Y. Zhi, C. Tang, Y. Bando, D. Golberg, B. Attal-Tretout, F. Ducastelle, and A. Loiseau, *Phys. Rev. B* **77**, 235422 (2008).
¹¹M. Terrones, W. K. Hsua, H. Terrones, J. P. Zhang, S. Ramos, J. P. Hare, R. Castillo, K. Prassides, A. K. Cheetham, H. W. Kroto, and D. R. M. Walton, *Chem. Phys. Lett.* **259**, 568 (1996).
¹²A. Loiseau, F. Willaime, N. Demoncey, G. Hug, and H. Pascard, *Phys. Rev. Lett.* **76**, 4737 (1996).
¹³D. Golberg, Y. Bando, M. Eremets, K. Takemura, K. Kurashima, and H. Yusa, *Appl. Phys. Lett.* **69**, 2045 (1996).
¹⁴D. P. Yu, X. S. Sun, C. S. Lee, I. Bello, S. T. Lee, H. D. Gu, K. M. Leung, G. W. Zhou, Z. F. Dong, and Z. Zhang, *Appl. Phys. Lett.* **72**, 1966 (1998).
¹⁵Y. Chen, L. T. Chadderton, J. FitzGerald, and J. S. Williams, *Appl. Phys. Lett.* **74**, 2960 (1999).
¹⁶H. Chen, Y. Chen, Y. Liu, H. Zhang, C. P. Li, Z. Liu, S. P. Ringer, and J. S. Williams, *Mater. Sci. Eng. B* **146**, 189 (2008).
¹⁷O. R. Lourie, C. R. Jones, B. M. Bartlett, P. C. Gibbons, R. S. Ruoff, and W. E. Buhro, *Chem. Mater.* **12**, 1808 (2000).
¹⁸C. Tang, Y. Bando, T. Sato, and K. Kurashima, *Chem. Commun.* **12**, 1290 (2002).
¹⁹C. Zhi, Y. Bando, C. Tan, and D. Golberg, *Solid State Commun.* **135**, 67 (2005).
²⁰F. H. Lin, C.-K. Hsu, T.-P. Tang, P.-L. Kang, F.-F. Yang, *Mater. Chem. Phys.* **107**, 115 (2008).
²¹W. Q. Han, Y. Bando, K. Kurashima, T. Sato, *Appl. Phys. Lett.* **73**, 3085 (1998).
²²C. H. Lee, J. Wang, V. K. Kayatsha, J. Y. Huang, and Y. K. Yap, *Nanotechnology* **19**, 455605 (2008).
²³L. Guo and R. N. Singh, *Phys. E* **41**, 448 (2009).
²⁴S. H. Lim, J. Luo, J. Wei, and J. Lin, *Catalysis Today* **120**, 346 (2007).
²⁵J.-Q. Bi, W.-L. Wang, Y.-X. Qi, Y.-J. Bai, L.-L. Pang, H.-L. Zhu, Y. Zhao, and Y. Wang, *Mater. Lett. B* **63**, 1299 (2009).
²⁶J. Yu, Y. Chen, and B. M. Cheng, *Solid State Commun. B* **149**, 763 (2009).
²⁷O. E. Alon, *Phys. Rev. B* **64**, 153408 (2001).

- ²⁸V. N. Popov, *Phys. Rev. B* **67**, 085408 (2003).
- ²⁹D. Sanchez-Portal and E. Hernandez, *Phys. Rev. B* **66**, 235415 (2002).
- ³⁰Y. Xiao, X. H. Yan, J. X. Cao, J. W. Ding, Y. L. L. Mao, and J. Xiang, *Phys. Rev. B* **69**, 205415 (2004).
- ³¹L. Wirtz, A. Rubio, R. A. de la Concha, and A. Loiseau, *Phys. Rev. B* **68**, 045425 (2003).
- ³²L. Wirtz and A. Rubio, *IEEE Trans. Nanotechnol.* **2**, 4 (2003).
- ³³B. Akdim, R. Pachter, X. Duan, and W. W. Adams, *Phys. Rev. B* **67**, 245404 (2003).
- ³⁴P. H. Lambin and J. P. Gaspard, *Phys. Rev. B* **26**, 4356 (1982), and references therein.
- ³⁵E. Jurczek, *Phys. Rev. B* **32**, 4208 (1985), and references therein.
- ³⁶C. Benoit, E. Royer, and G. Poussigue, *J. Phys. Condens. Matter* **4**, 3125 (1992).
- ³⁷C. Benoit, G. Poussigue, and A. Assaf, *J. Phys. Condens. Matter* **4**, 3153 (1992).
- ³⁸A. Rahmani, C. Benoit, and G. Poussigue, *J. Phys. Condens. Matter* **5**, 7941 (1993).
- ³⁹A. Rahmani, C. Benoit, R. Jullien, G. Poussigue, and A. Sakout, *J. Phys. Condens. Matter* **9**, 2149 (1997).
- ⁴⁰A. Rahmani, P. Jund, C. Benoit, and R. Jullien, *J. Phys. Condens. Matter* **13**, 5413 (2001).
- ⁴¹A. Rahmani, J.-L. Sauvajol, S. Rols, and C. Benoit, *Phys. Rev. B* **66**, 125404 (2002).
- ⁴²J.-L. Bantignies, J.-L. Sauvajol, A. Rahmani, and E. Flahaut, *Phys. Rev. B* **74**, 195425 (2006).
- ⁴³K. Sbai, A. Rahmani, H. Chadli, J.-L. Bantignies, P. Hermet, and J.-L. Sauvajol, *J. Phys. Chem. B* **110**, 12388 (2006).
- ⁴⁴K. Sbai, A. Rahmani, H. Chadli, and J.-L. Sauvajol, *J. Phys. Condens. Matter* **20**, 015204 (2008).
- ⁴⁵K. Sbai, A. Rahmani, H. Chadli, and J.-L. Sauvajol, *J. Phys. Condens. Matter* **21**, 045302 (2009).
- ⁴⁶J. Cambedouzou, J.-L. Sauvajol, A. Rahmani, E. Flahaut, A. Peigney, and C. Laurent, *Phys. Rev. B* **69**, 235422 (2004).
- ⁴⁷H. Chadli, A. Rahmani, K. Sbai, P. Hermet, S. Rols, J.-L. Sauvajol, *Phys. Rev. B* **74**, 205412 (2006).
- ⁴⁸A. Rahmani and H. Chadli, in *Handbook of Nanophysics: Structure and Vibrations in C60 Carbon Peapods* (Taylor and Francis, New York, 2010), p. 46.
- ⁴⁹B. Fakrach, A. Rahmani, H. Chadli, K. Sbai, and J.-L. Sauvajol, *Phys. E* **41**, 1800 (2009).
- ⁵⁰E. Rokuta, Y. Hasegawa, K. Suzuki, Y. Gamou, C. Oshima, and A. Nagashima, *Phys. Rev. Lett.* **79**, 4609 (1997).
- ⁵¹A. A. Maradudin, E. W. Montroll, G. H. Weiss, and I. P. Ipatova, *Theory of Lattice Dynamics in the Harmonic Approximation* (Academic, New York, 1971).
- ⁵²R. A. Jishi, L. Venkataraman, M. S. Dresselhaus, and G. Dresselhaus, *Chem. Phys. Lett.* **209**, 77 (1993).